AMERICAN SOCIETY FOR MICROBIOLOGY | Molecular and Cellular Biology®

RESEARCH ARTICLE

DHTKD1 Deficiency Causes Charcot-Marie-Tooth Disease in Mice

Wang-Yang Xu,[a,b] Houbao Zhu,[a] Yan Shen,[a] Ying-Han Wan,[b] Xiao-Die Tu,[b] Wen-Ting Wu,[b] Lingyun Tang,[a] Hong-Xin Zhang,[a,c] Shun-Yuan Lu,[a,c] Xiao-Long Jin,[d] Jian Fei,[b] Zhu-Gang Wang[a,b,c]

[a]State Key Laboratory of Medical Genomics, Research Center for Experimental Medicine of Rui-Jin Hospital, Shanghai Jiao Tong University School of Medicine, Shanghai, China

[b]Shanghai Research Center for Model Organisms, Shanghai, China

[c]Model Organism Division, E-Institutes of Shanghai Universities, Shanghai Jiao Tong University School of Medicine, Shanghai, China

[d]Department of Pathology, Rui-Jin Hospital, Shanghai Jiao Tong University School of Medicine, Shanghai, China

ABSTRACT DHTKD1, a part of 2-ketoadipic acid dehydrogenase complex, is involved in lysine and tryptophan catabolism. Mutations in *DHTKD1* block the metabolic pathway and cause 2-aminoadipic and 2-oxoadipic aciduria (AMOXAD), an autosomal recessive inborn metabolic disorder. In addition, a nonsense mutation in *DHTKD1* that we identified previously causes Charcot-Marie-Tooth disease (CMT) type 2Q, one of the most common inherited neurological disorders affecting the peripheral nerves in the musculature. However, the comprehensive molecular mechanism underlying CMT2Q remains elusive. Here, we show that *Dhtkd1*$^{-/-}$ mice mimic the major aspects of CMT2 phenotypes, characterized by progressive weakness and atrophy in the distal parts of limbs with motor and sensory dysfunctions, which are accompanied with decreased nerve conduction velocity. Moreover, DHTKD1 deficiency causes severe metabolic abnormalities and dramatically increased levels of 2-ketoadipic acid (2-KAA) and 2-aminoadipic acid (2-AAA) in urine. Further studies revealed that both 2-KAA and 2-AAA could stimulate insulin biosynthesis and secretion. Subsequently, elevated insulin regulates myelin protein zero (*Mpz*) transcription in Schwann cells via upregulating the expression of early growth response 2 (Egr2), leading to myelin structure damage and axonal degeneration. Finally, 2-AAA-fed mice do reproduce phenotypes similar to CMT2Q phenotypes. In conclusion, we have demonstrated that loss of DHTKD1 causes CMT2Q-like phenotypes through dysregulation of *Mpz* mRNA and protein zero (P_0) which are closely associated with elevated DHTKD1 substrate and insulin levels. These findings further indicate an important role of metabolic disorders in addition to mitochondrial insufficiency in the pathogenesis of peripheral neuropathies.

KEYWORDS DHTKD1, 2-aminoadipic acid, Charcot-Marie-Tooth disease, 2-aminoadipic and 2-oxoadipic aciduria, nerve conduction velocity

Dehydrogenase E1 and transketolase domain-containing protein 1 (DHTKD1) constitute the E1 subunit of the alpha-ketoadipic acid dehydrogenase complex. It has been considered to be involved in lysine and tryptophan catabolism (1, 2). The degradation of lysine and tryptophan within mitochondria forms the final product acetyl coenzyme A (acetyl-CoA), which participates in multiple mitochondrial functions. *DHTKD1* silencing leads to reduced mitochondrial biogenesis and impaired energy production (3). More importantly, the blockage of the metabolic pathway due to heterozygous or homozygous mutations in human *DHTKD1* leads to the accumulation of upstream substrates, resulting in alpha-aminoadipic and alpha-ketoadipic aciduria (AMOXAD) (1, 2, 4), which is an autosomal recessive inborn disorder of metabolism

Received 5 March 2018 **Returned for modification** 3 April 2018 **Accepted** 8 April 2018

Accepted manuscript posted online 16 April 2018

Citation Xu W-Y, Zhu H, Shen Y, Wan Y-H, Tu X-D, Wu W-T, Tang L, Zhang H-X, Lu S-Y, Jin X-L, Fei J, Wang Z-G. 2018. DHTKD1 deficiency causes Charcot-Marie-Tooth disease in mice. Mol Cell Biol 38:e00085-18. https://doi.org/10.1128/MCB.00085-18.

Address correspondence to Zhu-Gang Wang, zhugangw@shsmu.edu.cn.

W.-Y.X. and H.Z. contributed equally to this article.

characterized by increased urinary excretion of 2-ketoadipic acid (2-KAA) and 2-aminoadipic acid (2-AAA). It has a wide range of clinical manifestations, including neurological features, early-onset developmental delay, mental retardation, moderate metabolic acidosis, ataxia, seizures, hypotonia, and delayed motor development as well completely normal development (5, 6). Among these features, neurological abnormalities are the most common clinical manifestation although the pathological link between biochemical disorders and neurological symptoms is not clear.

We previously identified a nonsense mutation in exon 8 of *DHTKD1* which causes Charcot-Marie-Tooth disease type 2Q (CMT2Q) (7), an inherited neurological disorder affecting the peripheral nerves in the musculature. CMTs or distal hereditary motor-sensor neuropathies (HMSNs) genetically and clinically represent a highly heterogeneous set of disorders characterized by peripheral demyelination and axonal degeneration, with motor and sensory dysfunctions (8, 9). Clinically, CMT has two major phenotypic forms: CMT type 1 (a demyelinating form) and CMT type 2 (an axonal form) (10). CMT2 affects the axon and is characterized by distal muscle weakness and atrophy with mild sensory disturbance. The nonsense mutation almost eradicates DHTKD1 expression due to a nonsense-mediated mRNA decay (NMD) mechanism. However, comprehensive molecular portraits of *DHTKD1* mutation-caused peripheral neuropathy remain elusive.

Thus, we generated *Dhtkd1*$^{-/-}$ mice through routine homologous recombination. Using this model, we demonstrate a crucial role for EGR2/protein zero (P_0) signaling in the development of CMT2 and suggest a novel relationship between aberrant lysine catabolism and inherited peripheral neuropathy.

RESULTS

DHTKD1 deficiency leads to CMT2-like phenotypes in mice. The *Dhtkd1*$^{-/-}$ mice were generated by routine homologous recombination (see Fig. S1 in the supplemental material); they were born alive and fertile, and the distribution of genotypes among the littermates from heterozygote crosses followed a Mendelian inheritance pattern. To determine whether the mice lacking *Dhtkd1* reproduce CMT2Q-like phenotypes characterized by impaired motor function and sensory loss, we performed a rotarod test for evaluation of muscle strength and a treadmill test for exercise tolerance assessment. It was found that there was no statistical difference in behavior tests between wild-type (wt) and *Dhtkd1*$^{-/-}$ mice at the age of 6 weeks (data not shown). However, the same tests on 6-month-old mice revealed that both *Dhtkd1*$^{-/-}$ male and female mice tended to have significant decreases in retention time in the rotarod test (Fig. 1A) and in running distance in the treadmill test (Fig. 1B) compared with the performance of wt mice. These data indicate that DHTKD1 deficiency leads to weakened muscle strength and motor tolerance in mice. Meanwhile, *Dhtkd1*$^{-/-}$ mice appear to have reduced pain sensitivity, evidenced by a longer response time than that of wt mice to hot stimulus in a hot plate test (Fig. 1C), which is indicative of sensory impairment due to *Dhtkd1* deficiency. All of these data indicate that *Dhtkd1*$^{-/-}$ mice have not only impaired motor performance but also sensory abnormalities, thus phenotypically representing the clinical manifestations of human late-onset CMTs or HMSNs. However, there was no statistical difference in behavior tests between wt and *Dhtkd1*$^{+/-}$ mice at different time periods (data not shown). Axonal degeneration is one of the main features in many neurological disorders, including CMTs and other peripheral neuropathies, usually with irreversible clinical deficits (11). To determine whether motor and sensory dysfunction in *Dhtkd1*$^{-/-}$ mice is due to axonal nerve damage, we challenged the mice with acrylamide, an axonal neurotoxin that accelerates the progress of preexisting axonal degeneration (12). Before and 6 days after acrylamide treatment, 6-week-old mice were subjected to a rotarod test. As shown in Fig. 1D, the retention time of *Dhtkd1*$^{-/-}$ mice dramatically decreased after treatment with acrylamide, while there was no significant difference between wt and *Dhtkd1*$^{-/-}$ under basal conditions. In fact, most *Dhtkd1*$^{-/-}$ mice treated with acrylamide fell off the rotarod device even in the pretraining process.

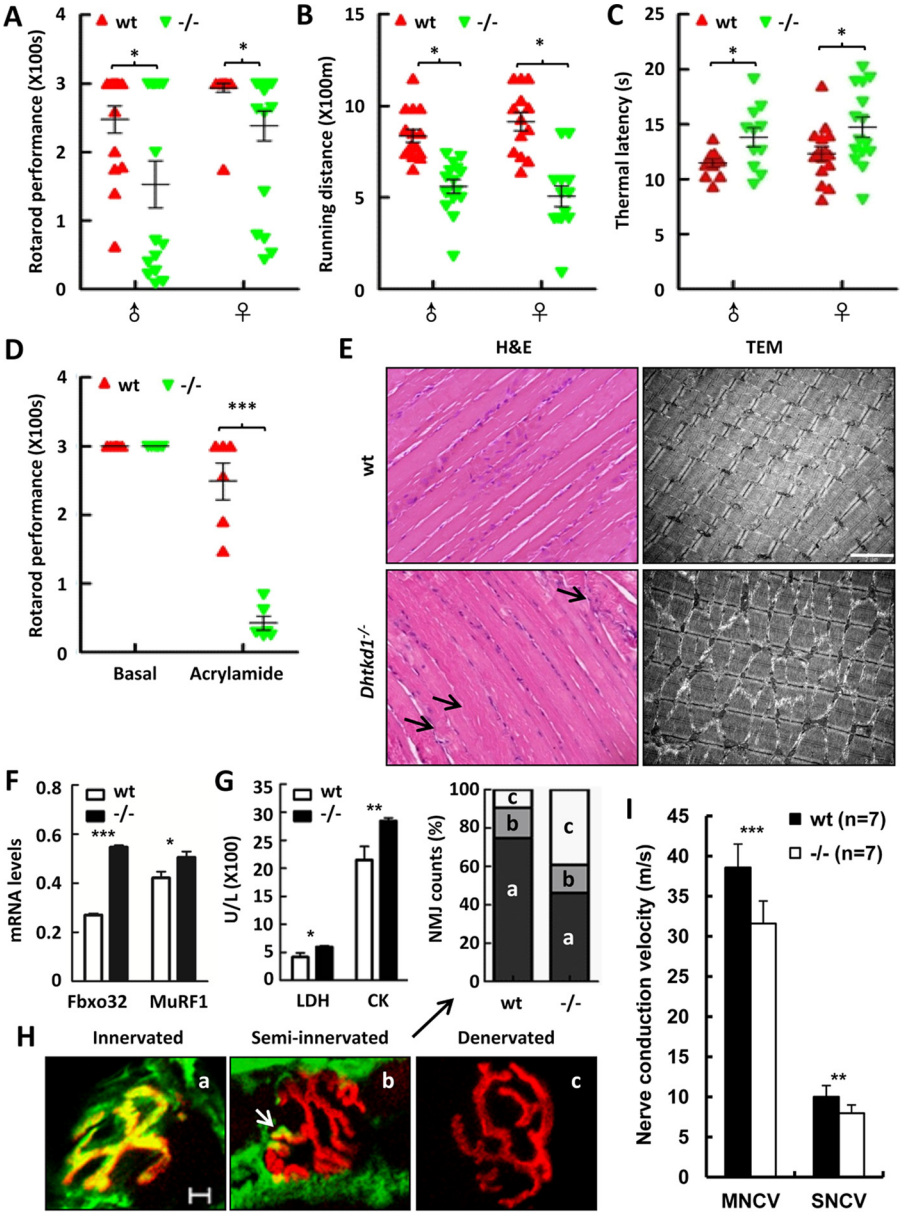

FIG 1 *Dhtkd1*$^{-/-}$ mice develop CMT2-like phenotypes. (A to C) Tests of general motor and sensory performance using an accelerating rotarod (A), a treadmill (B), and a hot plate test (C) ($n = 15$ mice per genotype). (D) When mice were exposed to 400 ppm of acrylamide for 6 days, retention time was assayed using an accelerating rotarod test ($n = 7$ mice per genotype). (E) H&E staining (left) denotes atrophies (arrows) in *Dhtkd1*$^{-/-}$ gastrocnemius muscle. Magnification, ×200. Electron microscopy (right) of the gastrocnemius sections in wt and *Dhtkd1*$^{-/-}$ mice shows sarcomere disorder in *Dhtkd1*$^{-/-}$ gastrocnemius muscle. Scale bar, 2 μm. (F) mRNA levels of atrophy-associated ubiquitin ligases, *Fbxo32* and *MuRF1*, detected by real-time PCR. (G) Circulating LDH and CK levels in serum ($n = 6$ mice per genotype). (H) Colocalization of alpha-bungarotoxin and SV2/SH3 markers indicates muscle innervations, partial colocalization representing semi-innervated junctions (arrow), and denervation as shown by alpha-bungarotoxin staining. On the basis of this classification, the percentages of innervated, semi-innervated, and denervated NMJ were analyzed by a chi-square test ($P < 0.001$). Scale bar, 5 μm. (I) Sciatic nerve conduction velocity. Values in panels A to D are shown as means ± SEM, while values shown in panels F, G, and I are shown as means ± SD. A Student two-sided *t* test was used for data in panels A to D, F, G, and I. *, $P < 0.05$; **, $P < 0.01$; ***, $P < 0.001$.

These data indicate that *Dhtkd1*$^{-/-}$ mice have axonal nerve damage, suggesting that DHTKD1 deficiency causes a CMT2-like phenotype in mice.

In addition, DHTKD1 deficiency indeed leads to muscle atrophy and sarcomere disorder or disappearance (Fig. 1E). Consistently, mRNA levels of atrophy-associated

ubiquitin ligase F-box protein 32 (*Fbxo32* product) and muscle RING finger 1 (*MuRF1* product) were found to be significantly elevated in the gastrocnemius of mice lacking DHTKD1
(Fig. 1F). Moreover, increased serum lactate dehydrogenase (LDH) and creatinine kinase (CK) levels were observed in *Dhtkd1*$^{-/-}$ mice (Fig. 1G). All of these findings suggest that muscular injury and atrophy occurred due to DHTKD1 deficiency. Additionally, abnormalities in the neuromuscular junctions (NMJs) have been confirmed in the development of neuropathies in several animal models (13–15). We found that *Dhtkd1*$^{-/-}$ mice have a pronounced increase in the percentage of denervated NMJs in gastrocnemius muscle compared with levels in wt mice (Fig. 1H). This suggests that the cause of progressive muscle weakness and atrophy in *Dhtkd1*$^{-/-}$ mice may be the nerve-muscle communication barrier. Electrophysiological analysis of sciatic nerves of 6-month-old mice showed that both motor nerve conduction velocity (MNCV) and sensory nerve conduction velocity (SNCV) decreased significantly in *Dhtkd1*$^{-/-}$ mice (Fig. 1I). Overall, *Dhtkd1*$^{-/-}$ mice anatomically and functionally develop peripheral neuropathy with obvious signs of motor and sensory impairment, axonal nerve degeneration, and muscle atrophy which resemble typical human CMT2Q phenotypes.

***Dhtkd1*$^{-/-}$ sciatic nerves display aberrant myelin structure with distal axonal loss due to abnormal P_0 expression.** To further characterize the CMT2-like phenotypes of *Dhtkd1*$^{-/-}$ mice, we used sciatic nerves as a window to look at the possible peripheral neuropathy due to DHTKD1 deficiency. It was clearly observed that the density of nerve fibers decreases, myelin sheath becomes irregular and dissociated from axons, and myelin sheath and axon degeneration occur in *Dhtkd1*-deficient sciatic nerves of 6-month-old mice (Fig. 2A). The morphological alterations of sciatic nerves and other tissues also seemed to be more severe in 30-week-old *Dhtkd1*$^{-/-}$ mice than in younger ones, suggesting a tendency of aggravation as *Dhtkd1*$^{-/-}$ mice age (Fig. S2). Morphometric analyses of the sections stained with toluidine blue further reveal reduced large myelinated fibers (>4 μm), loss of distal axons, and increased aberrant myelin with unchanged fiber area and thickness of the myelin sheath (Fig. 2B to F) in *Dhtkd1*$^{-/-}$ sciatic nerves. Since large myelinated fibers mainly represent motor neurons, this result suggests impaired motor capability. Schwann cells (SCs) play an important role in promoting axonal regeneration by producing neurotrophic factors such as nerve growth factor (NGF) and brain-derived neurotrophic factor (BDNF). We detected *Bdnf* and *Ngf* mRNA levels in sciatic nerve and found that they decreased in *Dhtkd1*$^{-/-}$ mice. However, the biomarker of Schwann cells, *S100b*, increased in *Dhtkd1*$^{-/-}$ sciatic nerves (Fig. 2G). These findings indicate that Schwann cells were functionally impaired in *Dhtkd1*$^{-/-}$ mice but that the number of Schwann cells increased. To understand why DHTKD1 deficiency causes peripheral neuropathy, we checked *Dhtkd1* expression in various tissues of mice (Fig. S3). It was found that *Dhtkd1* mRNA was expressed at higher levels in liver, kidney, spinal cord, dorsal root ganglia (DRG), mammary gland, and testes and at a lower level in the sciatic nerves, where DHTKD1 protein was restricted to S100-positive Schwann cells and not found in neurofilament-positive neurons (Fig. 2H). Thus, we proposed that DHTKD1 ablation in Schwann cells may directly affect the myelin sheath first and then subsequently affect axons and nerve conduction. To this end, we examined the expression levels of major myelin genes. The results showed a dramatic increase in *Mpz* (myelin protein zero) mRNA (Fig. 2I). Conversely, the expression of myelin structural proteins P_0 and myelin basic protein (MBP) in *Dhtkd1*$^{-/-}$ sciatic nerves decreased (Fig. 2J). EGR2 is a zinc finger transcription factor known to activate *Mpz* transcription synergistically with SOX10 in Schwann cells (16, 17). The level of EGR2 significantly increased in the sciatic nerves of *Dhtkd1*$^{-/-}$ mice (Fig. 2K and L), while there was no statistical difference in levels of SOX10 (data not shown). Further results showed that extracellular signal-regulated kinase 1 and 2 (ERK1/2) was activated in *Dhtkd1*$^{-/-}$ sciatic nerves (Fig. 2L), consistent with the previous findings of EGR2 activation depending on the MEK-ERK pathway (18). Thus, it seems that increased EGR2 activates the transcription of *Mpz*, which guides P_0 protein expression in a template dose-dependent way.

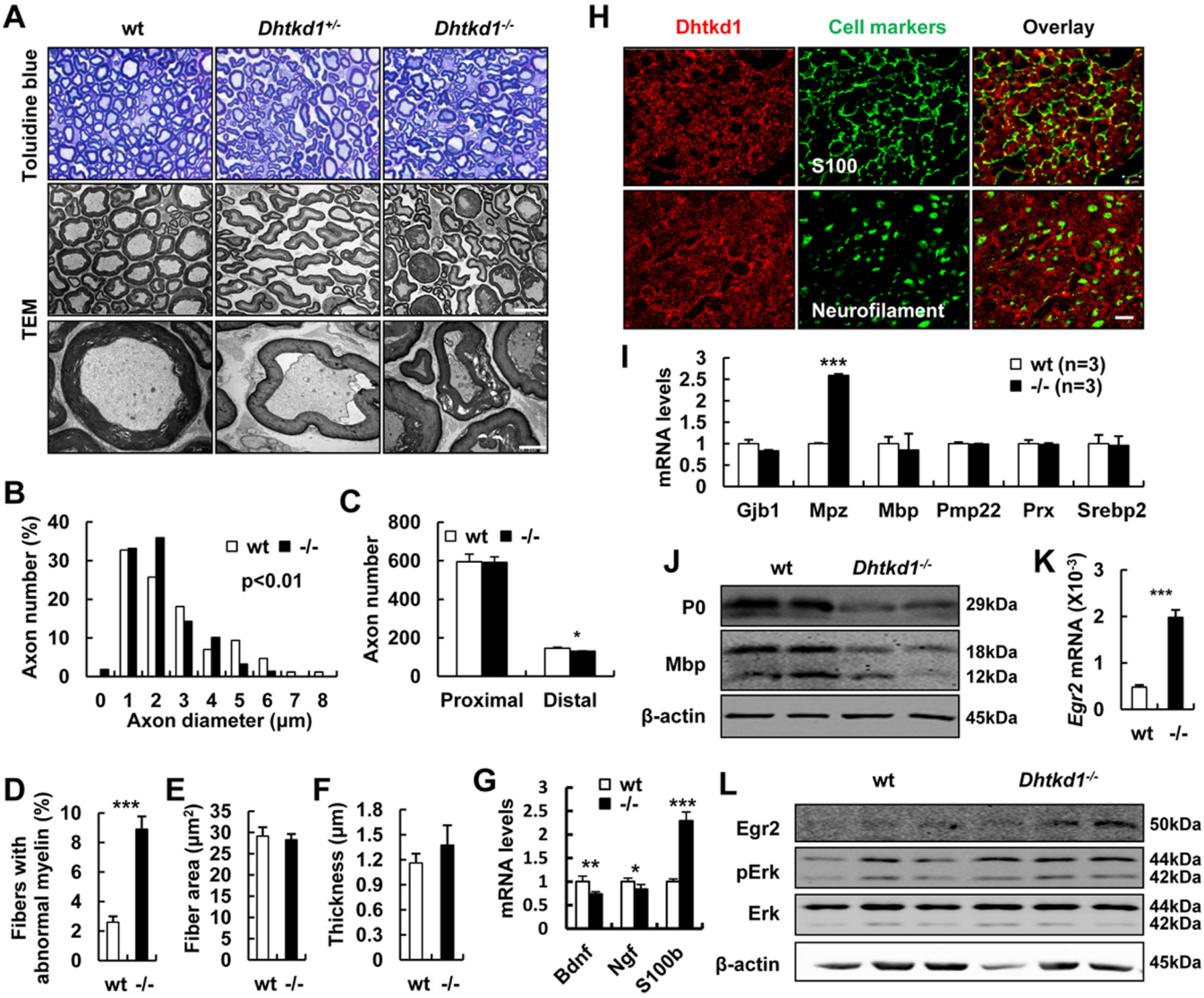

FIG 2 Aberrant myelin and axon morphology in *Dhtkd1*$^{-/-}$ sciatic nerves is caused by aberrant P_0 expression. (A) Semithin cross sections of sciatic nerves stained with toluidine blue. Magnification, ×1,000. Electron micrographs of sciatic nerves exhibit abnormal myelin fractures and axon degeneration in *Dhtkd1*$^{-/-}$ mice. Scale bars, 10 μm (middle panel) and 2 μm (bottom panel). (B) Chi-square test ($P = 0.003$) shows the distribution of axon diameters of the sciatic nerves. (C) Quantification of the number of axons in both proximal and distal parts of the sciatic nerves. (D) The percentage of irregular fiber (index of circularity < 0.75) in *Dhtkd1*$^{-/-}$ mice and in wt mice (3 mice with 15 fields per group). (E and F) Fiber area and myelin thickness are not changed due to *Dhtkd1* deletion. (G) Real-time PCR analysis shows the expression levels of *Bdnf*, *Ngf*, and *S100b*. (H) Expression of DHTKD1 on cryosections of sciatic nerves. Scale bar, 10 μm. (I) Real-time PCR analysis shows the expression levels of central myelin genes in sciatic nerves, including *Mpz*, myelin basic protein (*Mbp*), connexin 32 (*Gjb1*), the peripheral myelin protein 22-kDa gene (*PMP22*), periaxin (*Prx*), and sterol regulatory element binding protein 2 (*Srebp2*). (J) Western blot analysis of P_0 and MBP protein levels in sciatic nerves from both wt and *Dhtkd1*$^{-/-}$ mice. (K) Real-time PCR analysis of *Egr2* mRNA expression in sciatic nerves. (L) Western blot analysis of EGR2 protein levels and the ERK signaling pathway in sciatic nerves from both wt and *Dhtkd1*$^{-/-}$ mice. β-Actin was used as a loading control. A Student two-sided *t* test was used for data shown in panels C to G, I, and K. Values for all parameters are shown as means ± SD. *, $P < 0.05$; **, $P < 0.01$; ***, $P < 0.001$.

DHTKD1 deficiency leads to accumulation of 2-AAA and 2-KAA in mice. In addition to the observation above that the phenotype of *Dhtkd1*$^{-/-}$ mice clearly mimics that of CMT2Q, we found that urine 2-KAA levels reached 1,096.4 μg/ml in *Dhtkd1*$^{-/-}$ mice while it was only about 3.2 μg/ml in wt controls. The urine 2-AAA level in *Dhtkd1*$^{-/-}$ mice was also increased up to 120 times higher than that of wt controls (Fig. 3A). Recently, 2-AAA was suggested to be a marker of type 2 diabetes risk and a potential modulator of glucose homeostasis in humans (19). In accordance with that, we found that glycogen was significantly accumulated in *Dhtkd1*$^{-/-}$ liver (Fig. 3B). Elevated serum insulin levels under either fasting or refed conditions (Fig. 3C), as well

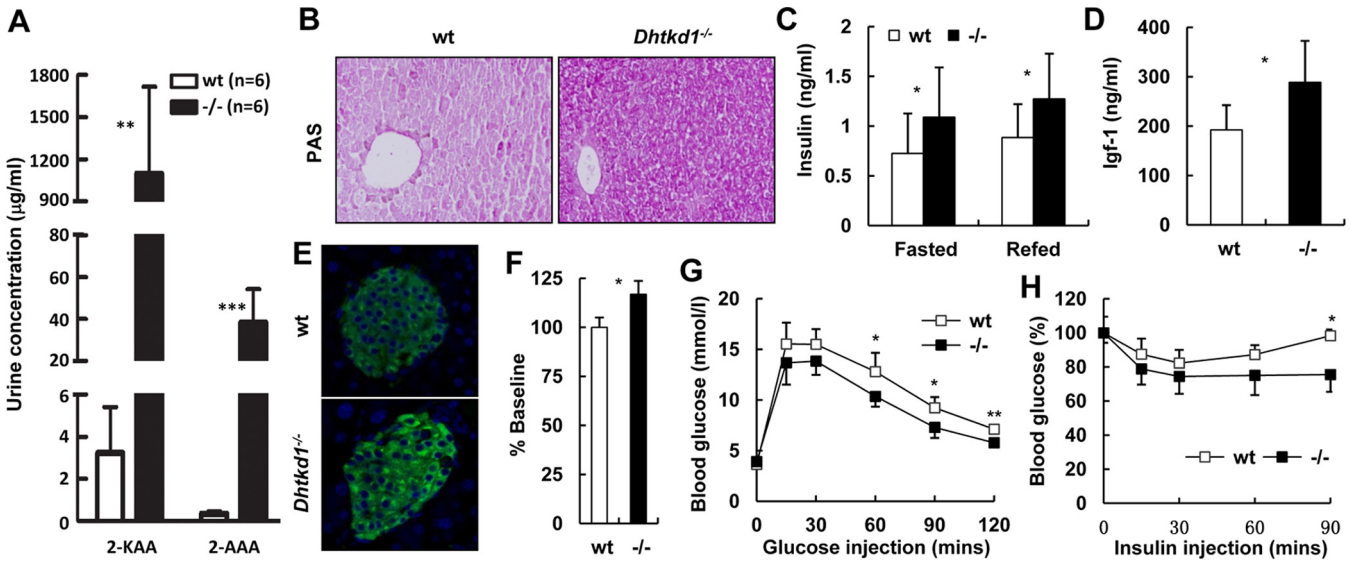

FIG 3 DHTKD1 deficiency leads to elevated insulin in mice. (A) GC/MS analysis of urinary excretion of 2-AAA and 2-KAA in 16-week-old mice. (B) Periodic acid-Schiff staining of glycogen in liver indicates more glycogen storage in *Dhtkd1*$^{-/-}$ liver. Magnification, ×200. (C) Serum insulin levels were measured (n = 10 mice per genotype). (D) *Dhtkd1*$^{-/-}$ mice exhibit increased plasma IGF-1 levels (n = 10 mice per genotype). (E) Immunofluorescence analysis of pancreatic insulin in islets shows elevated insulin in *Dhtkd1*$^{-/-}$ mice. Magnification, ×200. (F) ELISA of insulin in isolated islets. (G and H) GTT and ITT in wt and *Dhtkd1*$^{-/-}$ mice (n = 7 or 8 mice per genotype). A Student two-sided t test was used for data in panels A, C, D, F, G, and H. Values are shown as means ± SD. *, $P < 0.05$; **, $P < 0.01$; ***, $P < 0.001$.

as an increase in the level of serum insulin-like growth factor 1 (IGF-1), were detected in *Dhtkd1*$^{-/-}$ mice (Fig. 3D). In parallel with a high level of circulating insulin in *Dhtkd1*$^{-/-}$ mice, insulin in *Dhtkd1*$^{-/-}$ islets was found to be markedly elevated, as determined by immunostaining (Fig. 3E) and enzyme-linked immunosorbent assay (ELISA) (Fig. 3F). Furthermore, *Dhtkd1*$^{-/-}$ mice displayed increased glucose tolerance in an intraperitoneal (i.p.) glucose tolerance test (GTT) (Fig. 3G) and enhanced insulin sensitivity (Fig. 3H). We also found that the insulin levels were higher in *Dhtkd1*$^{-/-}$ mice than in wt mice during a GTT (Fig. S4). This demonstrates that lower glucose in *Dhtkd1*$^{-/-}$ mice is due to both increased insulin secretion (Fig. 3C and S4) and increased insulin sensitivity (Fig. 3H). Nevertheless, the observed lower glucose in an insulin tolerance test (ITT) might be due to an unexplored phenotype in the muscle and liver of the *Dhtkd1*$^{-/-}$ mice.

2-AAA and 2-KAA stimulate insulin biosynthesis and secretion *in vitro* and *in vivo*. To address the hypothesis that the elevated insulin level in *Dhtkd1*$^{-/-}$ mice is caused by increased 2-AAA or 2-KAA, we checked the responses of cultured mouse islets to 2-AAA and 2-KAA at different concentrations. The results showed that both 2-AAA (19) and 2-KAA stimulated wt islets to secrete insulin, and the responses were related to 2-AAA and 2-KAA doses (Fig. 4A). However, the histological structure of islets remained normal in *Dhtkd1*$^{-/-}$ mice (Fig. S5) although highly increased 2-AAA and 2-KAA levels existed. Moreover, positive effects of 2-AAA and 2-KAA on mouse islets were found for many functions (Fig. 4B to E), including insulin transcription (*Ins1* and *Ins2*), glucose uptake and metabolism (*Glut2*, *Gck*, and *Pcx*), insulin biosynthesis (*Ero1lb* and *Slc30a8*), and three different insulin secretion pathways (*Sytl4*, *Ucn3*, *Glp1r*, *Abcc*, *Kcnj11*, *Pclo*, and *Noc2*) (20). Additionally, serum insulin levels significantly increased in mice after exposure to 2-AAA for 8 weeks (Fig. 4F) (19), consistent with decreased fasting glucose levels (Fig. 4G). 2-AAA-fed mice had an improved glucose tolerance capacity compared to that of control mice (Fig. 4H), while insulin sensitivity was not affected (Fig. 4I). These data clearly indicate a positive effect of 2-AAA and 2-KAA on insulin biosynthesis and secretion.

Insulin regulates the myelin protein P_0 level in an EGR2-dependent manner. Insulin and its receptor could act as regulatory factors in the central and peripheral

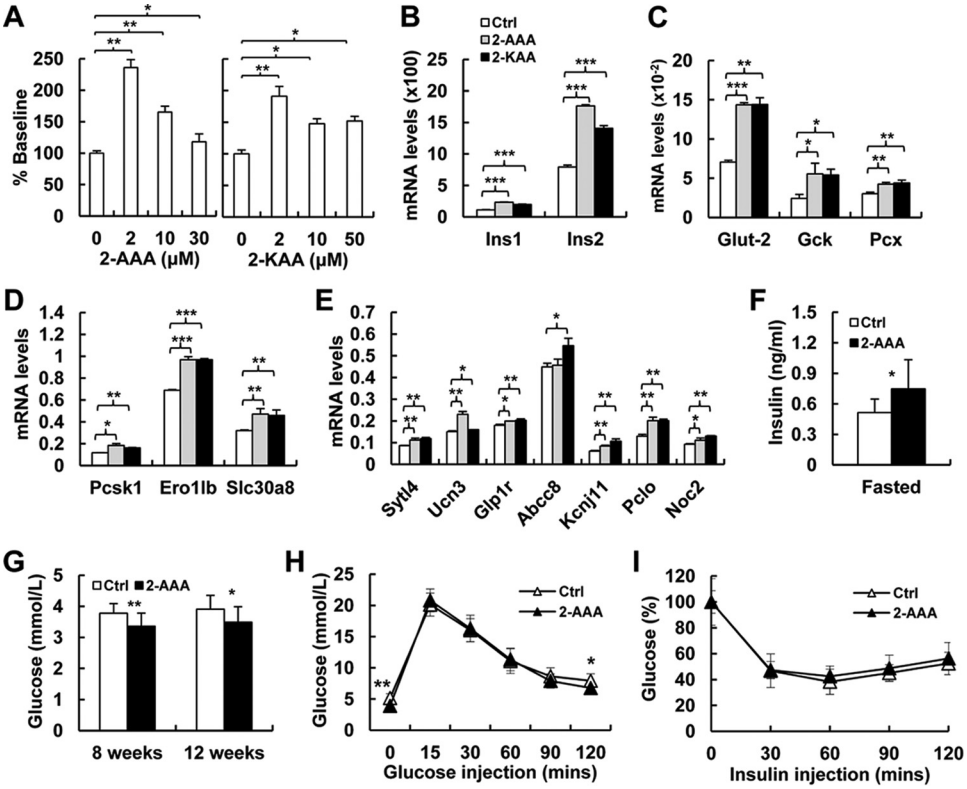

FIG 4 2-AAA and 2-KAA induce insulin biosynthesis and secretion *in vitro* and *in vivo*. (A) The effects of 2-AAA (19) and 2-KAA on insulin secretion in primary mouse islets from wt mice. (B) Real-time PCR analysis shows significant increases in *Ins1* and *Ins2* expression in *Dhtkd1*$^{-/-}$ islets treated with 2-AAA and 2-KAA. (C) Real-time PCR analysis of genes involved in glycolytic flux of islets treated with 2-AAA and 2-KAA. (D) Real-time PCR analysis of *Dhtkd1*$^{-/-}$ islets reveals increased expression of genes involved in insulin biosynthesis in 2-AAA- and 2-KAA-treated mice compared to levels in the wt. (E) Real-time PCR analysis of genes related to different insulin secretion pathways after 2-AAA and 2-KAA treatment shows elevated levels of these genes in *Dhtkd1*$^{-/-}$ islets. (F) Fasting plasma insulin was measured after 8 weeks of 2-AAA intake (2.5 mg/ml drinking water; $n = 9$ mice per group) (19). (G) Decreased fasting glucose levels in mice after 8 weeks and 12 weeks of 2-AAA intake are shown ($n = 9$ mice per group). (H) GTT was performed on 16-week-old control and 2-AAA-fed mice after 16 h of fasting using 2 g of glucose/kg body weight by i.p. injection. Plasma glucose levels during the GTT are presented. (I) ITT was performed on 6-h-fasted 16-week-old control and 2-AAA-fed mice with i.p. injection of insulin at 0.75 unit/kg body weight. Plasma glucose levels are presented as percent change from the glucose level at time zero. A Student two-sided *t* test was used, and values are shown as means ± SD. *, $P < 0.05$; **, $P < 0.01$; ***, $P < 0.001$.

nervous systems (21–24). MPZ mRNA and protein levels in SCs increase significantly in the presence of insulin (25). As shown above, DHTKD1 deficiency led to a marked increase in sciatic nerves in *Mpz* mRNA, which was activated by an elevated EGR2 expression level through the MEK-ERK signaling pathway (Fig. 2I to L). Thus, it is reasonable to question whether elevated insulin in *Dhtkd1*$^{-/-}$ mice contributes to the abnormal expression of *Mpz* and EGR2. To this end, we isolated Schwann cells from sciatic nerves of wt or *Dhtkd1*$^{-/-}$ mice and exposed cell cultures to different doses of insulin. The normal Schwann cells responded to insulin stimulation with dose-sensitive mRNA expression levels of both *Mpz* and *Egr2*. A significant increase in *Egr2* expression accompanied by *Mpz* expression was observed in primary SCs from wt mice grown in the presence of low insulin concentrations (Fig. 5A and B). In SCs incubated at higher insulin concentrations, the *Mpz* mRNA level decreased (Fig. 5A), presumably due to downregulation of the insulin receptor in SCs. This may be the reason why Schwann cells deficient for DHTKD1 appeared to lose such responses at the same dosage of insulin because *Egr2* and *Mpz* expression levels were exceedingly high in *Dhtkd1*$^{-/-}$ SCs under basal conditions (Fig. 5A and B). At the same time, expression levels of other myelin genes, such as *Mbp*, *Pmp22*, and *Srebp2*, did not change significantly

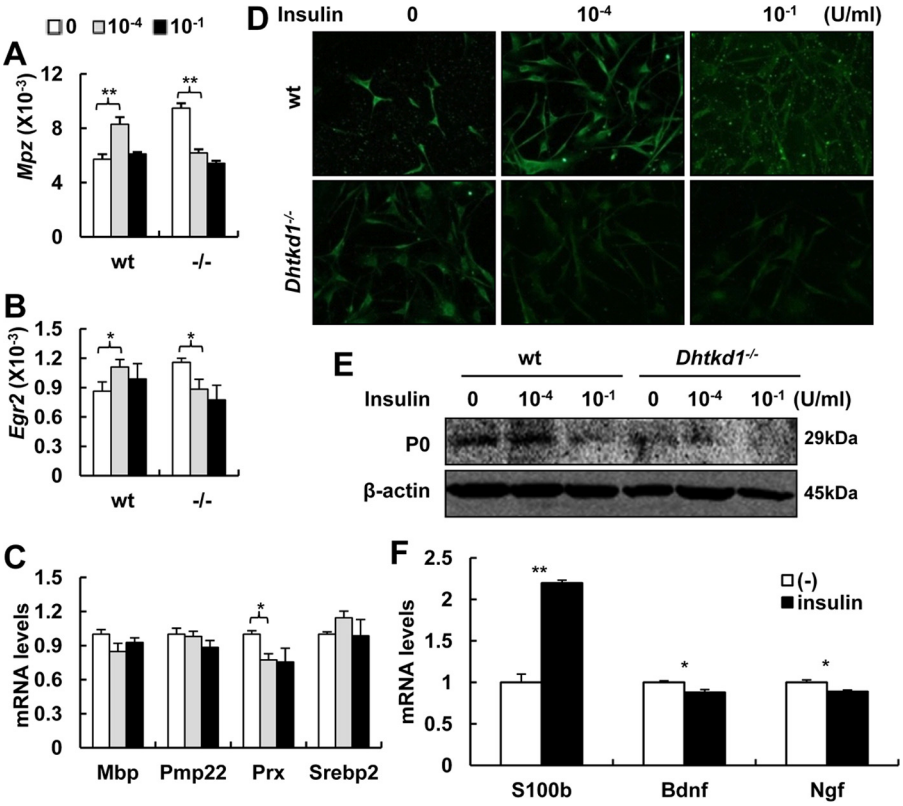

FIG 5 Insulin regulates myelin protein P_0 level in an EGR2-dependent manner. (A) The effect of insulin on *Mpz* expression in primary Schwann cells from both wt and *Dhtkd1*$^{-/-}$ mice. (B) The effect of insulin on *Egr2* mRNA expression. (C) Real-time PCR analysis of the expression patterns of other myelin genes after insulin treatment. (D and E) P_0 expression decreased with the increase of insulin concentrations, as assayed via immunofluorescence (D) and Western blotting (E). (F) Real-time PCR analysis of the expression *S100b*, *Bdnf*, and *Ngf*. A Student two-sided *t* test was used for data in panels A to C and F, and values are shown as means ± SD. *, $P < 0.05$; **, $P < 0.01$.

in conjunction with changes in insulin concentrations, suggesting that the *Mpz* gene might be the major object of insulin signaling in SCs although *Prx* was suppressed *in vitro* (Fig. 5C). We next checked P_0 expression in wt or *Dhtkd1*$^{-/-}$ Schwann cells in response to insulin stimulation. Similar to the *Mpz* mRNA response pattern, insulin positively regulated P_0 protein expression, especially at low doses in wt cells, but negatively suppressed the P_0 level at high doses in wt cells (Fig. 5D and E). These data suggest that a proper insulin level is crucial for normal expression of myelin protein P_0 and maintenance of the normal multilamellar structure of myelin in an EGR2-dependent manner. Furthermore, *Bdnf* and *Ngf* mRNA levels decreased, and *S100b* increased in the Schwann cells when they were cultured with insulin (10^{-4} U/ml) (Fig. 5F), suggesting that insulin contributes to the functional and quantitative impairment of Schwann cells.

2-AAA-fed mice develop CMT2-like phenotypes. Our data indicate that *Dhtkd1*$^{-/-}$ mice with elevated insulin levels induced by highly increased 2-AAA and 2-KAA develop peripheral neuropathy, suggesting that 2-AAA or 2-KAA may act as a key factor in triggering neurological processes. We then assigned some mice to receive 2-AAA (2.5 mg/ml) in drinking water for 4 months. Results show that 2-AAA-fed mice presented obvious abnormalities in motor performance or tolerance (Fig. 6A and B). Examination of semithin sections of sciatic nerves of 2-AAA-fed mice revealed aberrant myelinated nerve fibers, collapsed myelin structures, and obvious axon nerve damage (Fig. 6C). These observations were consistent with the myelin and axonal lesions seen in *Dhtkd1*$^{-/-}$ mouse models (Fig. 2A). Moreover, the *Mpz* mRNA level in sciatic nerves of 2-AAA-fed mice significantly increased (Fig. 6D), while P_0 and MBP levels in sciatic

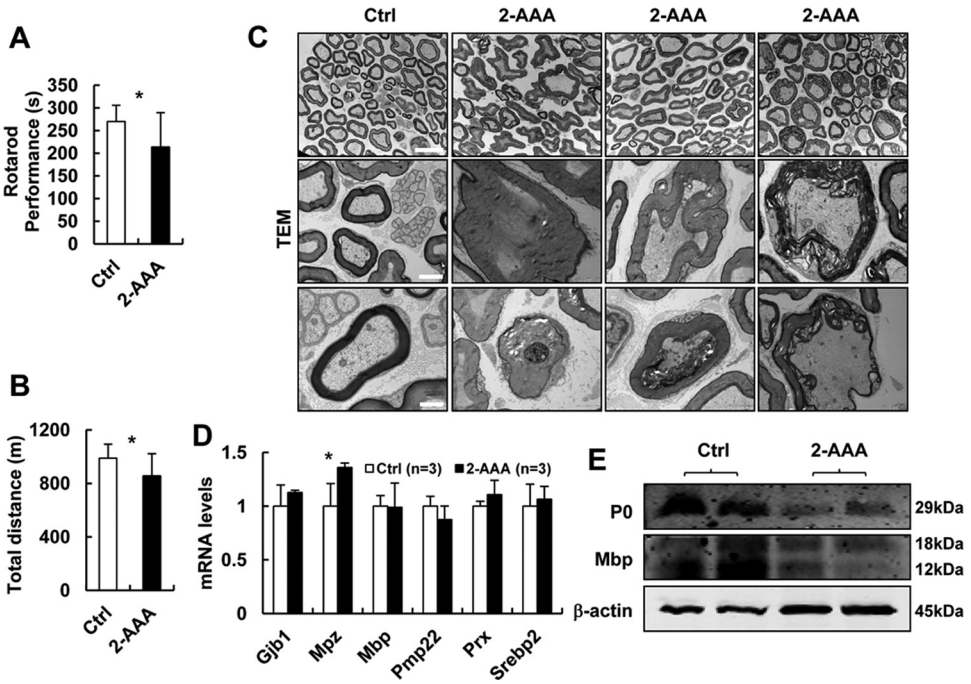

FIG 6 2-AAA-fed mice develop CMT2-like phenotypes similar to those of *Dhtkd1*$^{-/-}$ mice. (A and B) Tests of general motor performance using an accelerating rotarod (A) and a treadmill (B) ($n = 10$ mice per group). (C) Electron micrographs of sciatic nerves in mice. Scale bars, 10 μm (top panel) and 2 μm (middle and bottom panels). (D) Real-time PCR analysis of the expression levels of central myelin genes, including *Gjb1*, *Mpz*, *Mbp*, *PMP22*, *Prx*, and *Srebp2*, in sciatic nerves. (E) Western blot analysis of P_0 and MBP protein levels in sciatic nerves. A Student two-sided *t* test was used for data in panels A, B, and D, and values are shown as means ± SD. *, $P < 0.05$.

nerves reached significantly lower levels (Fig. 6E). *Dhtkd1* deficiency led to peripheral neuropathy, and the same clinical phenotypes and pathological changes occurred in 2-AAA-fed mice, indicating that 2-AAA has a pathogenic role in CMT2Q. To study the correlation between plasma insulin levels and phenotypes of peripheral nerves in 2-AAA-treated mice, we fed 1-month-old C57 mice with different concentrations of 2-AAA. One month later, we found that the pathological changes in sciatic nerves were closely connected with the plasma insulin levels (Fig. S6). These findings suggest the possible effect of insulin on promoting neuropathies of *Dhtkd1*$^{-/-}$ mice and 2-AAA-fed mice.

DISCUSSION

Mutations in *DHTKD1* result in increased urinary excretion of 2-KAA and 2-AAA (1). We previously identified a nonsense mutation in *DHTKD1* leading to CMT2Q peripheral neuropathy (7). To study the mechanism of *DHTKD1* mutation-caused CMT2Q, we produced *Dhtkd1* knockout mice. Our data show that *Dhtkd1*$^{-/-}$ mice develop severe peripheral neuropathy.

More comprehensive phenotype analyses revealed that *Dhtkd1*$^{-/-}$ mice display overt neurological phenotypes characterized by progressive weakness and atrophy in the distal parts of limbs, with motor impairments and sensory loss, mimicking the major aspects of human adult-onset axonal neuropathy, CMT2. The most notable changes in the sciatic nerves of *Dhtkd1*$^{-/-}$ mice were identified as developmental damage of myelin. These abnormalities are different from demyelination because Schwann cells can form myelin sheaths. It is known that the myelin sheath is crucial for the normal structure and impulse conduction of peripheral nerves, while the normal process of myelination of peripheral nerves depends on precisely regulated doses of a series of genes related to myelin structure (26, 27). *Mpz*, which is the most abundantly expressed gene in Schwann cells, encodes P_0, which mediates adhesion in the spiral wraps of the Schwann cell's myelin sheaths. It has been recognized as a critical component in the

compaction and maintenance of the multilamellar structure of myelin sheath (28, 29). Mutations in *MPZ* would destroy myelination and even disrupt the interaction between axon and myelin, causing neuropathies in adulthood (30–33). The dosage of *MPZ* mRNA must be precisely regulated because either genetic defects in *MPZ* or an increase in gene dosage may cause congenital peripheral neuropathies, such as CMT diseases (27, 34, 35). Moreover, studies on various lines of *MPZ* transgenic mice have suggested that P_0 overexpression causes dysmyelinating neuropathy with obviously delayed nerve development (36). Interestingly, P_0 protein level is not always consistent with the *Mpz* mRNA expression level because an increased protein level is detected only in the nerve tissues with low *Mpz* mRNA overexpression (36). Researchers suggested that as *Mpz* dosage rises, increasing *Mpz* overexpression dysregulates the stoichiometric expression of other myelin genes to cause the destruction of myelin structures in progressively impaired Schwann cells, leading to destabilization and degradation of myelin proteins (33, 37). Similarly, *Dhtkd1*$^{-/-}$ mice have a dramatic increase in *Mpz* mRNA and decreases in P_0 and MBP proteins in sciatic nerves and cultured Schwann cells (Fig. 2I and J and 5A, D, and E). Why *Mpz* mRNA is highly upregulated in the absence of DHTKD1 could be ascribed to the elevated expression level of EGR2 (Fig. 2K and L), a zinc finger transcription factor known to activate *Mpz* transcription in Schwann cells (16, 17). Moreover, elevated serum IGF-1, possibly due to hypoglycemia, in *Dhtkd1*$^{-/-}$ mice may also contribute to the upregulation of *Mpz* expression in an EGR2-dependent manner (16). However, the question of how elevated *Mpz* mRNA is linked to reduced P_0 protein expression in *Dhtkd1*$^{-/-}$ mice remains to be further addressed.

2-AAA has been suggested as a possible diabetes risk factor (19). Individuals with a high 2-AAA concentration had greater than a 4-fold risk of developing diabetes for many years to come. In addition, individuals with high 2-AAA levels are associated with lower fasting glucose levels and BMIs. After chronic administration of 2-AAA, the highest 2-AAA level was found in the pancreas alone, along with high insulin levels, suggesting a close connection between 2-AAA and elevated insulin levels *in vivo* (19). Based on this clue and the fact that hyperinsulinemia and highly accumulated 2-AAA and 2-KAA simultaneously exist in *Dhtkd1*$^{-/-}$ mice (Fig. 3), we performed extensive analyses on the potential role of these metabolites in facilitating insulin biosynthesis and secretion and subsequent effects on glucose homeostasis. Either 2-AAA or 2-KAA stimulates mouse islets to secrete insulin, and the responses are related to 2-AAA and 2-KAA doses (Fig. 4A). Moreover, 2-AAA and 2-KAA facilitate the transcriptional expression of insulin and the genes associated with glucose uptake and metabolism, insulin biosynthesis, and insulin secretion pathways to some degree (Fig. 4B to E). The serum insulin level of mice administered 2-AAA significantly increased (Fig. 4F). These *in vitro* and *in vivo* data strongly suggest that 2-AAA and 2-KAA highly accumulated in *Dhtkd1*$^{-/-}$ mice and may contribute to the development of an elevated insulin level. Numerous observations highlight the effect of insulin on the pathogenesis of neuropathies, such as Alzheimer's disease and peripheral neuropathies with severe myelin alterations. The cultured Schwann cells positively respond to insulin stimulation in the transcriptional expression of *Mpz* and *Egr2* in a dose-dependent manner. Taking these observations together, it seems reasonable to believe that the inevitable intrinsic defects in Schwann cells due to DHTKD1 deficiency as well as hyperinsulinemia jointly contribute to the collapse of myelin proteins, leading to peripheral neuropathy. However, it would be interesting to know whether increased metabolites affect myelin protein expression directly because some inherited disorders of amino acid degradation present a severe clinical phenotype caused by toxicity of accumulating metabolites. AMOXAD patients with *DHTKD1* mutations manifest rather mild phenotypes. The reason might be that missense mutations in *DHTKD1* retain residual protein function or a lower toxicity of accumulating metabolites, just as with another *Dhtkd1* knockout mouse model (38). This model mimicked mild clinical phenotypes in AMOXAD patients which were different from the clinical manifestations in our *Dhtkd1*$^{-/-}$ mice. Completely different targeting strategies may be responsible for this difference because the mouse of the

previous study harbored a 431-amino-acid-truncated protein while our mouse was targeted at exons 2 to 4, and it was only possible to generate a 55-amino-acid peptide. Though complete loss of function in *Dhtkd1*$^{-/-}$ mice leads to more severe metabolic and neurological phenotypes, we suppose that phenotypes observed in *Dhtkd1*$^{-/-}$ mice are closely related to the toxicity of accumulating metabolites.

In conclusion, our data suggest that DHTKD1 deficiency leads to adult-onset axonal peripheral neuropathy. Furthermore, increased 2-AAA and 2-KAA facilitate insulin biosynthesis and secretion and subsequently lead to abnormal expression of myelin protein EGR2/P_0, critical for the wrapping of myelin. These observations together provide a novel connection between metabolic disorder and inherited peripheral neuropathy.

MATERIALS AND METHODS

Animal models. The *Dhtkd1*$^{-/-}$ mice were generated by routine homologous recombination (see Fig. S1 in the supplemental material) and were maintained on a C57BL/6 background under specific-pathogen-free conditions and free access to water and diet unless otherwise specified. All procedures were approved by the Animal Ethics Committee of Rui-Jin Hospital. Unless otherwise noted, only male mice were used in this study.

Mouse behavioral testing. For a rotarod test, mice were trained for 2 days at a constant speed of 20 rpm for 300 s per mouse. On the third day, mice were tested at 20 rpm, and the times of retention were recorded. The test was terminated if the retention time was more than 300 s. For the group of acrylamide-treated mice, 6-week-old mice were treated with 400 ppm of acrylamide (Sigma) in drinking water for 6 days before training. For the treadmill test, the voltage of the electric shock device was set to 50 V. The test was divided into the adaptation and testing phases. During the adaptation phase, the belt speed was 5 m/min, and the belt angle was 0°. After 5 min of adaptation, mice were placed in the runway. The belt speed was raised to 20 m/min (3 m/min every 15 min), and the angle of the belt slowly increased to 12° (3° per 15 min). The total movement distance of each mouse was recorded. For a thermal latency test, timed latency to hind limb withdrawal was assessed at 52°C. All the behavioral tests were executed in a double-blind fashion.

Electrophysiological analysis. Mice were anesthetized with chloral hydrate (0.3 g/kg) and placed in a thermostatic blanket to keep their body temperatures at 37 ± 0.5°C. When the plantar and corneal reflex disappeared, the nerve conduction velocity was measured. For MNCV, two stimulation electrodes (terminal diameter, 0.25 mm) were inserted into the sciatic notch (SN) and Achilles tendon (AT), and the recording electrode (terminal diameter, 0.25 mm) was inserted into interosseous muscle. The stimulation current was 4 mA, and the duration was 100 μs. The compound muscle action potential (M wave) and H reflex (Hoffman's reflex) were collected by the signal collector after being converted and amplified 1,000 times. MNCV is calculated as the distance between SN and AT/the latency difference of the M wave peak induced by the stimulation sites at SN and AT, respectively. For SNCV, the stimulation electrode was inserted into the second toe nerve, and the recording electrode was inserted into the Achilles tendon. The stimulation current was 1.5 times the threshold of sensory nerve-evoked potential, and the duration was 20 μs. The sensory nerve A/C-fiber-evoked potential was collected by the signal collector after being converted and amplified 2,000 times. SNCV is calculated as the distance between the toe tip and AT/the latency of the evoked potential.

Mouse Schwann cell culture and stimulation. Schwann cell culture was performed as previously reported (39). Six-week-old mice were sacrificed, and sciatic nerves were removed, stripped, and cultured in Dulbecco's modified Eagle's medium (DMEM)–F-12 (1:1) medium (Gibco) supplemented with 20% fetal bovine serum, 2 μg/ml bovine pituitary extract (Gibco), 100 μg/ml streptomycin, and 100 units/ml penicillin at 37°C in a 5% humidified CO_2 atmosphere. The medium was changed every 2 days. After 1 week, the sciatic nerves were cut into pieces and digested with 0.25% trypsin and 0.1% collagenase II for 30 min at 37°C. Then the tissues were scattered, washed, and resuspended in medium. Cells were dispersed in 35-mm culture dishes and transferred into poly-L-lysine-coated dishes after 30 min. Three days later, the cells were digested with 0.25% trypsin. When the majority of Schwann cells detached, digestion was stopped, and the detached cells were collected. Then the cells were seeded into poly-L-lysine-coated six-well plates or 18-mm coverslips at a density of 2×10^5 cells/ml. The cells were cultured in the aforementioned medium supplemented with different concentrations of insulin and harvested after 72 h.

Mouse islet isolation and stimulation. Islets were isolated from 3-month-old mouse pancreas by collagenase digestion, according to a previously reported method (19, 40), separated by Ficoll density gradient centrifugation, picked by hand, and then cultured for 24 h in 1640 medium (HyClone) containing 10% fetal bovine serum. Ten islets were transferred into each microcentrifuge tube and incubated in 1 ml of islet secretion buffer (120 mmol/liter NaCl, 5 mmol/liter KCl, 1 mmol/liter $CaCl_2$, 1.2 mmol/liter $MgCl_2$, 24 mmol/liter $NaHCO_3$, 10 mmol/liter HEPES, and 2.5 mmol/liter glucose), with or without 5 μM 2-AAA or 2-KAA, for 6 h at 37°C and 5% CO_2. Insulin level was assayed using a mouse insulin ELISA kit (Mercodia). Islets were extracted with 0.18 N HCl in 70% ethanol for determination of insulin content, and secretion was normalized to islet insulin content.

Urine 2-KAA and 2-AAA detection. Urine and standard 2-KAA and 2-AAA (Sigma) first underwent derivatization with propyl chloroformate for 24 h at room temperature to yield derivatives for gas

chromatography-mass spectrometry (GC/MS) analysis. Then the GC/MS analysis was performed using a GC/MS QP2010 Plus instrument (Shimadzu) at Shanghai Institute of Materia Medica.

Western blot analysis. Tissues or cells were lysed in lysis buffer, and proteins were separated by SDS-PAGE, transferred to nitrocellulose membranes, and probed with specific antibodies (3, 41). Antibodies used were the following: mouse anti-DHTKD1 (Abnova), goat anti-MPZ (Abnova), goat anti-MBP (Santa Cruz), rabbit anti-glyceraldehyde-3-phosphate dehydrogenase (anti-GAPDH) (Sangon Biotech), rabbit anti-EGR2 (Sigma),and rabbit anti-β-actin, anti-ERK, and anti-pERK (Cell Signaling Technology [CST]).

Serum biochemical analysis. Mouse blood samples taken from retrobulbar veins were centrifuged, and the sera were analyzed using an automatic biochemical analyzer. Blood insulin and IGF-1 contents were detected through ELISAs according to the manufacturer's instructions using a mouse insulin ELISA kit (Mercodia) and IGF-1 ELISA kit (Abnova), respectively.

Intraperitoneal glucose tolerance test (GTT). Four-month-old mice were fasted overnight for 16 h and were injected intraperitoneally with 2 g of glucose/kg body weight. Blood from the tail vein was collected at 0, 15, 30, 60, 90, and 120 min after injection. Blood glucose levels were measured with a glucometer (Sinocare).

Insulin tolerance test (ITT). Four-month-old mice were fasted for 6 h and intraperitoneally injected with 0.75 U/kg human insulin (Humulin; Lilly). Tail blood samples were collected at 0, 30, 60, 90, and 120 min after injection. Blood glucose levels were measured with a glucometer (Sinocare).

Quantitative reverse transcription-PCR (qRT-PCR). Total RNA was isolated with TriPure reagent (Roche) and then reverse transcribed into cDNA with a reverse transcriptase reagent kit with genomic DNA (gDNA) eraser (TaKaRa). Quantitative PCR was carried out with a SYBR green PCR kit (TaKaRa). Amplifications were performed in a Mastercycler ep realplex instrument (Eppendorf). Relative transcript quantities were calculated using the ΔC_T (where C_T is threshold cycle) method with the β-actin gene as the reference gene. Each sample was analyzed in triplicate. Primers were designed using DNAMAN software or obtained from PrimerBank (42), and the sequences are listed in Table S1.

Immunocytochemistry. Livers were dissected and fixed in 10% formalin and sectioned for Dhtkd1 immunohistochemistry. Sections were deparaffinized, antigen unmasked, blocked routinely, incubated with primary Dhtkd1 antibody (Abnova), and developed with a streptavidin-horseradish peroxidase (HRP) system. Sciatic nerves were dissected quickly and frozen into liquid nitrogen with optimal-cutting-temperature (OCT) compound. Sections were blocked and incubated with specific primary antibodies, including goat anti-DHTKD1 (Santa Cruz), rabbit anti-S100β (Santa Cruz), and rabbit antineurofilament (ThermoFisher). Sections were washed the following day and incubated with secondary antibodies. For NMJ staining, skeletal muscles were dissected and fixed in cold 2% paraformaldehyde overnight and then embedded in 3% agarose and sectioned into 100-μm-thick sections with a vibratome. Sections were incubated overnight in a primary antibody mixture of mouse anti-neurofilament 2H3 and anti-SV2 (Developmental Studies Hybridoma Bank), washed the following day, and incubated with Alexa Fluor 488-conjugated anti-mouse antibody and Alexa Fluor 594-conjugated alpha-bungarotoxin (Invitrogen). Cultured Schwann cells were fixed, permeated, blocked routinely, incubated with primary MPZ antibody (Proteintech), and developed with Alexa Fluor 488-conjugated anti-rabbit antibody. Pancreas sections were stained with polyclonal guinea pig anti-insulin (Dako) and developed with Alexa Fluor 488-conjugated anti-guinea pig antibody (Life Technology).

Histopathology analysis. Skeletal muscles were isolated and fixed in 10% formalin and sectioned. Hematoxylin and eosin (H&E) staining was performed routinely. For transmission electron microscopy (TEM), mice were perfused with 2.5% glutaraldehyde under anesthesia. Then the skeletal muscles, sciatic nerves, and spinal cords were quickly dissected and fixed in 2.5% glutaraldehyde. Semithin sections were stained with toluidine blue, and the TEM was carried out using a Philips CM120 instrument at Shanghai Jiao Tong University School of Medicine.

Statistical analyses. All quantitative data shown as histograms are presented as means $\pm$ standard deviations (SD), and those shown as scatter plots are presented as means $\pm$ standard errors of the means (SEM). A two-tailed Student *t* test was used to analyze the differences between two groups. A chi-square test was used to analyze the distribution differences of NMJ and axons between two groups. A *P* value of <0.05 was considered to be statistically significant.

SUPPLEMENTAL MATERIAL

Supplemental material for this article may be found at https://doi.org/10.1128/MCB.00085-18.

SUPPLEMENTAL FILE 1, PDF file, 1.3 MB.

ACKNOWLEDGMENTS

We thank D. Chen of the Shanghai Institute of Materia Medica for technical support in urine KAA and AAA detection and X. Wang of Rui-Jin Hospital for technical support in mouse islet isolation.

This research was supported partially by grants from the National Natural Science Foundation of China (81430028, 81201365, and 81502048), the Ministry of Science and Technology of China (2011BAI15B02), the Science and Technology Commission of Shanghai Municipality (13DZ2280600, 13DZ2293700, and 15DZ2290800), the E-Institutes of

Shanghai Municipal Education Commission (E03003), and the Research Award Fund for Outstanding Young Teachers from the Shanghai Education Commission (ZZjdyx12108).

REFERENCES

1. Danhauser K, Sauer SW, Haack TB, Wieland T, Staufner C, Graf E, Zschocke J, Strom TM, Traub T, Okun JG, Meitinger T, Hoffmann GF, Prokisch H, Kolker S. 2012. DHTKD1 mutations cause 2-aminoadipic and 2-oxoadipic aciduria. Am J Hum Genet 91:1082–1087. https://doi.org/10.1016/j.ajhg.2012.10.006.
2. Hagen J, te Brinke H, Wanders RJ, Knegt AC, Oussoren E, Hoogeboom AJ, Ruijter GJ, Becker D, Schwab KO, Franke I, Duran M, Waterham HR, Sass JO, Houten SM. 2015. Genetic basis of alpha-aminoadipic and alpha-ketoadipic aciduria. J Inherit Metab Dis 38:873–879. https://doi.org/10.1007/s10545-015-9841-9.
3. Xu W, Zhu H, Gu M, Luo Q, Ding J, Yao Y, Chen F, Wang Z. 2013. DHTKD1 is essential for mitochondrial biogenesis and function maintenance. FEBS Lett 587:3587–3592. https://doi.org/10.1016/j.febslet.2013.08.047.
4. Stiles AR, Venturoni L, Mucci G, Elbalalesy N, Woontner M, Goodman S, Abdenur JE. 2016. New Cases of DHTKD1 mutations in patients with 2-ketoadipic aciduria. JIMD Rep 25:15–19. https://doi.org/10.1007/8904_2015_462.
5. Fischer MH, Brown RR. 1980. Tryptophan and lysine metabolism in alpha-aminoadipic aciduria. Am J Med Genet 5:35–41. https://doi.org/10.1002/ajmg.1320050106.
6. Przyrembel H, Bachmann D, Lombeck I, Becker K, Wendel U, Wadman SK, Bremer HJ. 1975. Alpha-ketoadipic aciduria, a new inborn error of lysine metabolism; biochemical studies. Clin Chim Acta 58:257–269. https://doi.org/10.1016/0009-8981(75)90445-3.
7. Xu WY, Gu MM, Sun LH, Guo WT, Zhu HB, Ma JF, Yuan WT, Kuang Y, Ji BJ, Wu XL, Chen Y, Zhang HX, Sun FT, Huang W, Huang L, Chen SD, Wang ZG. 2012. A nonsense mutation in DHTKD1 causes Charcot-Marie-Tooth disease type 2 in a large Chinese pedigree. Am J Hum Genet 91:1088–1094. https://doi.org/10.1016/j.ajhg.2012.09.018.
8. Barisic N, Claeys KG, Sirotkovic-Skerlev M, Lofgren A, Nelis E, De Jonghe P, Timmerman V. 2008. Charcot-Marie-Tooth disease: a clinico-genetic confrontation. Ann Hum Genet 72:416–441. https://doi.org/10.1111/j.1469-1809.2007.00412.x.
9. Zuchner S, Vance JM. 2006. Mechanisms of disease: a molecular genetic update on hereditary axonal neuropathies. Nat Clin Pract Neurol 2:45–53. https://doi.org/10.1038/ncpneuro0071.
10. Pareyson D, Scaioli V, Laura M. 2006. Clinical and electrophysiological aspects of Charcot-Marie-Tooth disease. Neuromolecular Med 8:3–22. https://doi.org/10.1385/NMM:8:1-2:3.
11. Krajewski KM, Lewis RA, Fuerst DR, Turansky C, Hinderer SR, Garbern J, Kamholz J, Shy ME. 2000. Neurological dysfunction and axonal degeneration in Charcot-Marie-Tooth disease type 1A. Brain 123:1516–1527. https://doi.org/10.1093/brain/123.7.1516.
12. Ewaleifoh O, Trinh M, Griffin JW, Nguyen T. 2012. A novel system to accelerate the progression of nerve degeneration in transgenic mouse models of neuropathies. Exp Neurol 237:153–159. https://doi.org/10.1016/j.expneurol.2012.05.021.
13. Baloh RH, Strickland A, Ryu E, Le N, Fahrner T, Yang M, Nagarajan R, Milbrandt J. 2009. Congenital hypomyelinating neuropathy with lethal conduction failure in mice carrying the Egr2 I268N mutation. J Neurosci 29:2312–2321. https://doi.org/10.1523/JNEUROSCI.2168-08.2009.
14. Dequen F, Filali M, Lariviere RC, Perrot R, Hisanaga S, Julien JP. 2010. Reversal of neuropathy phenotypes in conditional mouse model of Charcot-Marie-Tooth disease type 2E. Hum Mol Genet 19:2616–2629. https://doi.org/10.1093/hmg/ddq149.
15. d'Ydewalle C, Krishnan J, Chiheb DM, Van Damme P, Irobi J, Kozikowski AP, Vanden Berghe P, Timmerman V, Robberecht W, Van Den Bosch L. 2011. HDAC6 inhibitors reverse axonal loss in a mouse model of mutant HSPB1-induced Charcot-Marie-Tooth disease. Nat Med 17:968–974. https://doi.org/10.1038/nm.2396.
16. LeBlanc SE, Jang SW, Ward RM, Wrabetz L, Svaren J. 2006. Direct regulation of myelin protein zero expression by the Egr2 transactivator. J Biol Chem 281:5453–5460. https://doi.org/10.1074/jbc.M512159200.
17. Topilko P, Schneider-Maunoury S, Levi G, Baron-Van Evercooren A, Chennoufi AB, Seitanidou T, Babinet C, Charnay P. 1994. Krox-20 controls myelination in the peripheral nervous system. Nature 371:796–799. https://doi.org/10.1038/371796a0.
18. Keeton AB, Bortoff KD, Bennett WL, Franklin JL, Venable DY, Messina JL. 2003. Insulin-regulated expression of Egr-1 and Krox20: dependence on ERK1/2 and interaction with p38 and PI3-kinase pathways. Endocrinology 144:5402–5410. https://doi.org/10.1210/en.2003-0592.
19. Wang TJ, Ngo D, Psychogios N, Dejam A, Larson MG, Vasan RS, Ghorbani A, O'Sullivan J, Cheng S, Rhee EP, Sinha S, McCabe E, Fox CS, O'Donnell CJ, Ho JE, Florez JC, Magnusson M, Pierce KA, Souza AL, Yu Y, Carter C, Light PE, Melander O, Clish CB, Gerszten RE. 2013. 2-Aminoadipic acid is a biomarker for diabetes risk. J Clin Invest 123:4309–4317. https://doi.org/10.1172/JCI64801.
20. Taylor BL, Liu FF, Sander M. 2013. Nkx6.1 is essential for maintaining the functional state of pancreatic beta cells. Cell Rep 4:1262–1275. https://doi.org/10.1016/j.celrep.2013.08.010.
21. Freychet P. 2000. Insulin receptors and insulin actions in the nervous system. Diabetes Metab Res Rev 16:390–392. https://doi.org/10.1002/1520-7560(200011/12)16:6<390::AID-DMRR161>3.0.CO;2-T.
22. Shetter AR, Muttagi G, Sagar CB. 2011. Expression and localization of insulin receptors in dissociated primary cultures of rat Schwann cells. Cell Biol Int 35:299–304. https://doi.org/10.1042/CBI20100523.
23. Sugimoto K, Murakawa Y, Sima AA. 2002. Expression and localization of insulin receptor in rat dorsal root ganglion and spinal cord. J Peripher Nerv Syst 7:44–53. https://doi.org/10.1046/j.1529-8027.2002.02005.x.
24. Sugimoto K, Murakawa Y, Zhang W, Xu G, Sima AA. 2000. Insulin receptor in rat peripheral nerve: its localization and alternatively spliced isoforms. Diabetes Metab Res Rev 16:354–363. https://doi.org/10.1002/1520-7560(200009/10)16:5<354::AID-DMRR149>3.0.CO;2-H.
25. Shettar A, Muttagi G. 2012. Developmental regulation of insulin receptor gene in sciatic nerves and role of insulin on glycoprotein P0 in the Schwann cells. Peptides 36:46–53. https://doi.org/10.1016/j.peptides.2012.04.012.
26. Greenfield S, Brostoff S, Eylar EH, Morell P. 1973. Protein composition of myelin of the peripheral nervous system. J Neurochem 20:1207–1216. https://doi.org/10.1111/j.1471-4159.1973.tb00089.x.
27. Yin X, Kidd GJ, Wrabetz L, Feltri ML, Messing A, Trapp BD. 2000. Schwann cell myelination requires timely and precise targeting of P_0 protein. J Cell Biol 148:1009–1020. https://doi.org/10.1083/jcb.148.5.1009.
28. Eichberg J. 2002. Myelin P0: new knowledge and new roles. Neurochem Res 27:1331–1340. https://doi.org/10.1023/A:1021619631869.
29. Menichella DM, Arroyo EJ, Awatramani R, Xu T, Baron P, Vallat JM, Balsamo J, Lilien J, Scarlato G, Kamholz J, Scherer SS, Shy ME. 2001. Protein zero is necessary for E-cadherin-mediated adherens junction formation in Schwann cells. Mol Cell Neurosci 18:606–618. https://doi.org/10.1006/mcne.2001.1041.
30. Giese KP, Martini R, Lemke G, Soriano P, Schachner M. 1992. Mouse P_0 gene disruption leads to hypomyelination, abnormal expression of recognition molecules, and degeneration of myelin and axons. Cell 71:565–576. https://doi.org/10.1016/0092-8674(92)90591-Y.
31. Nelis E, Haites N, Van Broeckhoven C. 1999. Mutations in the peripheral myelin genes and associated genes in inherited peripheral neuropathies. Hum Mutat 13:11–28. https://doi.org/10.1002/(SICI)1098-1004(1999)13:1<11::AID-HUMU2>3.0.CO;2-A.
32. Shy ME. 2006. Peripheral neuropathies caused by mutations in the myelin protein zero. J Neurol Sci 242:55–66. https://doi.org/10.1016/j.jns.2005.11.015.
33. Warner LE, Hilz MJ, Appel SH, Killian JM, Kolodry EH, Karpati G, Carpenter S, Watters GV, Wheeler C, Witt D, Bodell A, Nelis E, Van Broeckhoven C, Lupski JR. 1996. Clinical phenotypes of different MPZ (P0) mutations may include Charcot-Marie-Tooth type 1B, Dejerine-Sottas, and congenital hypomyelination. Neuron 17:451–460. https://doi.org/10.1016/S0896-6273(00)80177-4.
34. Hoyer H, Braathen GJ, Eek AK, Skjelbred CF, Russell MB. 2011. Charcot-Marie-Tooth caused by a copy number variation in myelin protein zero. Eur J Med Genet 54:e580–583. https://doi.org/10.1016/j.ejmg.2011.06.006.
35. Maeda MH, Mitsui J, Soong BW, Takahashi Y, Ishiura H, Hayashi S, Shirota Y, Ichikawa Y, Matsumoto H, Arai M, Okamoto T, Miyama S, Shimizu J, Inazawa J, Goto J, Tsuji S. 2012. Increased gene dosage of myelin protein

zero causes Charcot-Marie-Tooth disease. Ann Neurol 71:84–92. https://doi.org/10.1002/ana.22658.
36. Wrabetz L, Feltri ML, Quattrini A, Imperiale D, Previtali S, D'Antonio M, Martini R, Yin X, Trapp BD, Zhou L, Chiu SY, Messing A. 2000. P_0 glycoprotein overexpression causes congenital hypomyelination of peripheral nerves. J Cell Biol 148:1021–1034. https://doi.org/10.1083/jcb.148.5.1021.
37. Kirschner DA, Szumowski K, Gabreels-Festen AA, Hoogendijk JE, Bolhuis PA. 1996. Inherited demyelinating peripheral neuropathies: relating myelin packing abnormalities to P0 molecular defects. J Neurosci Res 46:502–508.
38. Biagosch C, Ediga RD, Hensler SV, Faerberboeck M, Kuehn R, Wurst W, Meitinger T, Kolker S, Sauer S, Prokisch H. 2017. Elevated glutaric acid levels in Dhtkd1-/Gcdh- double knockout mice challenge our current understanding of lysine metabolism. Biochim Biophys Acta 1863:2220–2228. https://doi.org/10.1016/j.bbadis.2017.05.018.
39. Zhu J, Qin J, Shen Z, Kretlow JD, Wang X, Liu Z, Jin Y. 2012. Dispase rapidly and effectively purifies Schwann cells from newborn mice and adult rats. Neural Regen Res 7:256–260. https://doi.org/10.3969/j.issn.1673-5374.2012.04.003.
40. Deng R, Nie A, Jian F, Liu Y, Tang H, Zhang J, Zhang Y, Shao L, Li F, Zhou L, Wang X, Ning G. 2014. Acute exposure of beta-cells to troglitazone decreases insulin hypersecretion via activating AMPK. Biochim Biophys Acta 1840:577–585. https://doi.org/10.1016/j.bbagen.2013.10.021.
41. Zhu H, Xu WY, Hu Z, Zhang H, Shen Y, Lu S, Wei C, Wang ZG. 2017. RNA virus receptor Rig-I monitors gut microbiota and inhibits colitis-associated colorectal cancer. J Exp Clin Cancer Res 36:2. https://doi.org/10.1186/s13046-016-0471-3.
42. Spandidos A, Wang X, Wang H, Seed B. 2010. PrimerBank: a resource of human and mouse PCR primer pairs for gene expression detection and quantification. Nucleic Acids Res 38:D792–D799. https://doi.org/10.1093/nar/gkp1005.